

Photoinduced Energy-Level Realignment at Interfaces between Organic Semiconductors and Metal-Halide Perovskites

Fengshuo Zu,¹ Jonathan H. Warby,² Martin Stolterfoht,² Jinzhao Li,³ Dongguen Shin¹,
Eva Unger,³ and Norbert Koch^{1,3,*}

¹*Institut für Physik & IRIS Adlershof, Humboldt-Universität zu Berlin, 12489 Berlin, Germany*

²*Institut für Physik und Astronomie, Universität Potsdam, 14776 Potsdam, Germany*

³*Helmholtz-Zentrum Berlin für Materialien und Energie GmbH, 12489 Berlin, Germany*

 (Received 1 April 2021; revised 19 June 2021; accepted 2 November 2021; published 8 December 2021)

In contrast to the common conception that the interfacial energy-level alignment is affixed once the interface is formed, we demonstrate that heterojunctions between organic semiconductors and metal-halide perovskites exhibit huge energy-level realignment during photoexcitation. Importantly, the photoinduced level shifts occur in the organic component, including the first molecular layer in direct contact with the perovskite. This is caused by charge-carrier accumulation within the organic semiconductor under illumination and the weak electronic coupling between the junction components.

DOI: [10.1103/PhysRevLett.127.246401](https://doi.org/10.1103/PhysRevLett.127.246401)

The relative positions of valence and conduction levels of two semiconductors forming a heterojunction, i.e., the energy-level alignment, is key for the junction's functionality in a device. It is accepted understanding that the energy-level alignment at a semiconductor heterojunction is fixed once it has been fabricated, unless—of course—physical and chemical changes occur due to ageing or degradation. Under device operation, typically involving biasing, current flow, and photon absorption or emission, deviations from the ground state energy-level situation are likely to occur. For instance, due to interfacial space-charge accumulation energy-level bending away from the interface is expected. This occurs—depending on the specific materials—on the nanometer to micrometer length scale. However, the level alignment at the very interface, i.e., where the two semiconductors directly touch on the atomic length scale, is considered fixed nonetheless. This can be readily understood for junctions with covalent and/or ionic bonds between the two materials, as is the case for most elemental and compound semiconductor junctions. This conception has been readily expanded to junctions formed by materials with weaker (van der Waals type) interfacial interactions, such as many organic semiconductors and metal-halide perovskites (MHPs). Interfaces of these two material classes have become particularly important in the recent past due to the remarkable progress made in perovskite photovoltaics [1–4], meanwhile reaching a power conversion efficiency (PCE) of over 25% for single junction cells [5]. In high-performance MHP-based solar cells charge-selective charge transport layers must be employed, and these are often organic semiconductors [2,6–11]. Here, the relative position of the perovskite's valence or conduction band maximum or minimum and the corresponding organic's frontier energy levels, i.e., highest

occupied molecular orbital (HOMO) and lowest unoccupied molecular orbital (LUMO) levels, determines the device performance [6,12–14]. As for every semiconductor heterojunction, the alignment of occupied energy levels at the MHP or charge transport layer interfaces can be directly determined by ultraviolet photoelectron spectroscopy (UPS) measurements [6,15–21]. However, it was pointed out that an accurate valence band (VB) onset of MHPs can only be determined by using a logarithmic photoemission intensity scale [16,17], and possible surface band bending due to surface states must be carefully considered [22,23].

Nonetheless, the persistence of a fixed interfacial energy-level offset determined for MHP or organic semiconductor junctions in the electronic ground state (in dark) also during device operation (under illumination) was never questioned. Here, we demonstrate that our view of energy levels at such interfaces has to be expanded. We determined the energy-level alignment at interfaces between the state-of-the-art triple cation perovskite $\text{Cs}_{0.05}[(\text{FAPbI}_3)_{0.83}(\text{MAPbBr}_3)_{0.17}]_{0.95}$ and organic semiconductors with charge-selective character, in dark and under solar irradiation. UPS measurements show that the energy levels of the organic layers significantly and reversibly shift, with respect to the Fermi level of the conductive substrate, under visible light compared to the dark state. In contrast, those of the perovskite layer do not. Photogenerated electron-hole pairs within the perovskite layer are efficiently separated at the MHP or organic semiconductor interface, resulting in the accumulation of electrons or holes within the electron- or hole-selective organic layer. Remarkably, even the energy levels of the organic molecules in direct contact with the perovskite exhibit this photoinduced space charge dependent realignment, whereas the energy levels of the perovskite remain

essentially unaffected. These observations, supported by model photovoltaic device data, evidence the breakdown of the common assumption that the energy-level alignment at a semiconductor heterojunction remains constant once the interface is formed, also under device operation conditions.

Details of sample preparation and experimental methods are given in the Supplemental Material [24]. To illustrate the effect of charge accumulation on the interfacial energy-level alignment upon exposing a MHP or organic junction to solar light, we first chose 1,4,5,8,9,12-hexazatriphenylenehexacarbonitrile (HATCN) as an electron transport material (ETL) because of its high electron affinity (>4.9 eV and up to 5.4 eV have been reported [29,30]). We combine HATCN with the triple cation perovskite $\text{Cs}_{0.05}[(\text{FAPbI}_3)_{0.83}(\text{MAPbBr}_3)_{0.17}]_{0.95}$ (abbreviated as CsFAMA), deposited on poly(3,4-ethylenedioxythiophene):polystyrene sulfonate (PEDOT:PSS) as a conductive substrate. The CsFAMA thin film on PEDOT:PSS (initial work function of 5.09 eV), exhibits a work function (Φ) of 5.05 eV in dark, as seen from the secondary electron cutoff (SECO) in Fig. 1(a), indicating essentially vacuum-level alignment at the interface, i.e., the absence of interface dipoles and/or band bending.

The VB onset for this CsFAMA film is determined on a logarithmic intensity scale to be 0.69 eV below the Fermi level of the conductive substrate (E_F), as shown in Fig. S1 in the Supplemental Material [24]. Accordingly, the conduction band (CB) onset is projected to lie 0.94 eV above E_F , by adding the material's band gap of 1.63 eV [31]. We did not observe surface photovoltage effects for PEDOT:PSS/CsFAMA upon light exposure (intensity equivalent to 1.5 sun), indicating flat band conditions throughout the perovskite layer and at the interface with PEDOT:PSS. Next, HATCN with a nominal thickness of 7 nm was deposited onto CsFAMA without breaking ultrahigh vacuum. We note that the nominal film thickness was determined with a quartz crystal microbalance, thus corresponding to a mass thickness. After HATCN deposition the sample Φ increased to 5.43 eV. This is accompanied by slight upward surface band bending in CsFAMA by 0.14 eV, as observed from the shift of the Pb 4*f* core levels by x-ray photoelectron spectroscopy (XPS) measurements in Fig. 1(c). The cause is most likely due to a small ground state electron transfer from ubiquitous CsFAMA gap states to HATCN [32,33]. Consequently, the perovskite VB onset must shift by the same amount as the core levels, from 0.69 (bare surface) to 0.55 eV after HATCN deposition. In the valence region [Fig. 1(b)], the HOMO onset of the 7 nm HATCN layer is determined to be at 3.85 eV on a linear intensity scale, per convention used in the organic electronics community [34–36]. This HOMO onset value is in agreement with other studies on HATCN films in the LUMO Fermi-level pinning regime [37,38], and thus consistent with the above-mentioned ground state charge transfer. Correspondingly, the LUMO level onset of

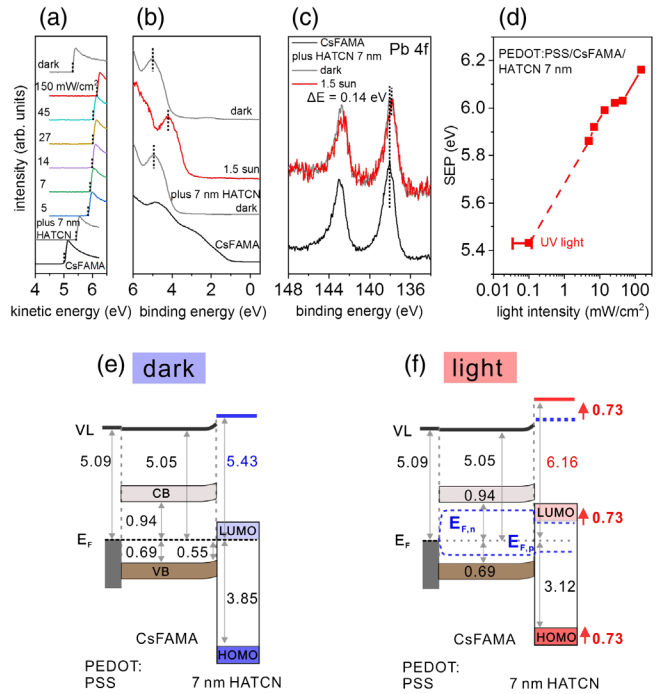


FIG. 1. Ultraviolet photoemission spectra of PEDOT:PSS/CsFAMA/7 nm HATCN measured in dark and under simulated solar irradiation, as indicated for the (a) secondary electron cutoff (SECO), (b) valence, and (c) Pb 4*f* core level regions. (d) Sample surface electrostatic potential (SEP) measured with respect to the conductive substrate Fermi level (E_F) as function of irradiation intensity. Schematic energy-level diagrams (e) in the dark and (f) under 1.5 sun irradiation. VL is the vacuum level. The indicated energy values are given with respect to E_F set to zero. The blue dashed lines in (f) represent the quasi-Fermi levels $E_{F,n}$ and $E_{F,p}$ for electrons and holes, respectively; the red arrows and numbers indicate the illumination-induced change of the HATCN energy levels with respect to those of the perovskite.

HATCN is essentially at E_F . The energy-level alignment at the CsFAMA/HATCN(7 nm) interface in the dark is displayed in Fig. 1(e) and corresponds to a type-II heterojunction with a large energy offset of 0.94 eV for electron extraction from CsFAMA to HATCN.

Subsequently, UPS measurements under varied illumination intensities were performed, as included in Figs. 1(a) and 1(b). The valence levels of HATCN exhibit an irradiation induced displacement towards E_F by up to 0.73 eV at 1.5 sun light intensity, and they return to the original (dark) position upon switching the light off. In parallel to the valence levels, the sample surface electrostatic potential (SEP) with respect to E_F of the conductive substrate increases logarithmically with light intensity, by up to 0.73 eV at 1.5 sun, as obtained by SECO measurements and summarized in Fig. 1(d). Note, in dark and under equilibrium the SEP corresponds to the sample work function Φ . In Fig. 1(d) we estimated the UV intensity (used to excite the photoelectrons) being equivalent to approximately 0.1 mW/cm², in analogy to a previously

reported photovoltage study using visible and UV light [23]. Also the SEP reverts to its initial value after switching the light off. In contrast, the energy levels of the perovskite remain unchanged during illumination, as seen from the constant Pb 4*f* core levels position with respect to E_F in Fig. 1(c). A detailed description of the measurement procedures to assess the SEP and all energy levels is given in the Supplemental Material [24]. The facts that only the HATCN levels shift reversibly, in parallel with the SEP, points to an underlying mechanism of an electrostatic nature. This comprises (i) photogeneration of carriers in the perovskite layer, (ii) subsequent electron transfer to the HATCN layer, where (iii) the free electrons accumulate. This electrostatic mechanism implies that all energy levels of HATCN (including HOMO, LUMO, vacuum level) shift in parallel with respect to those of the underlying perovskite, i.e., the HATCN ionization energy and electron affinity remain unchanged.

So far, we accessed only the photoinduced shift of the topmost molecular layer of 7 nm (multilayer) thick HATCN due to the surface sensitivity of UPS, and one might expect that the energy-level alignment at the very interface between CsFAMA and HATCN remains unchanged under illumination, and that the negative space-charge accumulated within the HATCN layer leads to upward energy-level bending within the organic layer. To obtain information about the energy levels of the first molecular layer in direct contact with the perovskite, HATCN with a nominal thickness of 0.4 nm was deposited onto the CsFAMA film. This thickness corresponds to ca. one monolayer of flat-lying molecules or submonolayer if the molecules are vertically inclined. The HATCN (sub)monolayer deposition increases the sample Φ slightly from 5.10 (bare CsFAMA) to 5.17 eV [Fig. 2(a)], again suggesting a small ground state electron transfer to HATCN. In the valence region [Fig. 2(b)], the apparent emission from the HATCN HOMO level peaking at ca. 4.7 eV is observed, superimposed on the emission from the perovskite underneath. To better visualize the spectral contribution from the molecular layer, an appropriately scaled bare CsFAMA spectrum was subtracted. From this, also shown in Fig. 2(b) and labeled “BGS,” the HATCN HOMO onset is determined at 3.51 eV below E_F .

Therefore, the position of the LUMO levels of neutral HATCN molecules is estimated accordingly at ca. 0.3 eV above E_F . The small density of electrons transferred to the molecules to reach the electronic ground state [39,40] appears as weak emission with a peak at ca. 1.4 eV and an onset at 0.79 eV below E_F , as clearly seen in the zoomed plot of Fig. 2(c). This emission feature is assigned to originate from the former LUMO (of the neutral molecule) that is split into two sublevels due to the electron transfer, with the singly occupied molecular orbital of the anion ($\text{SOMO}_{\text{anion}}$) level below E_F and its unoccupied counterpart above [41]. In addition, the former HOMO of neutral

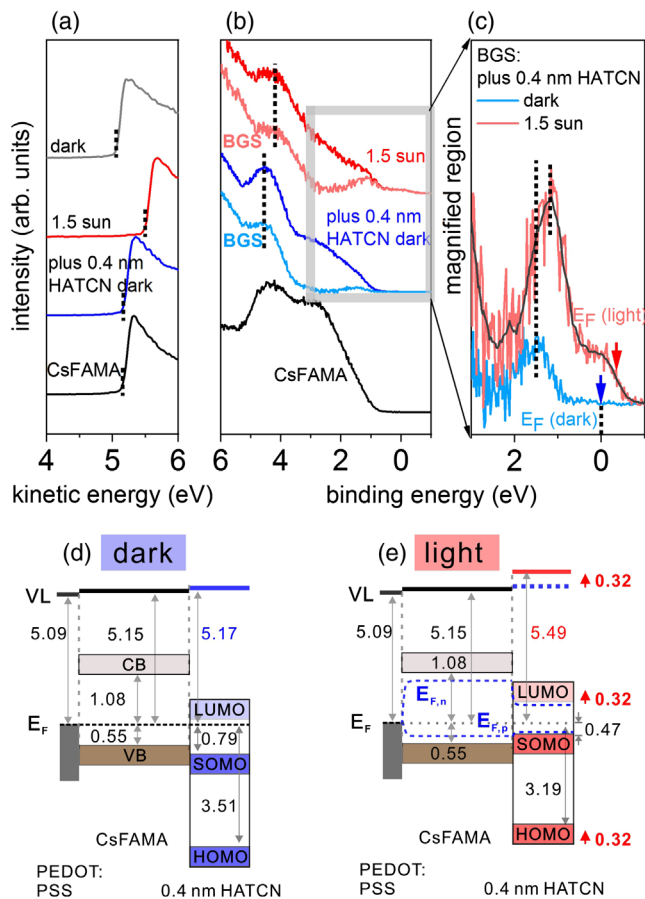


FIG. 2. Ultraviolet photoemission spectra of PEDOT:PSS/CsFAMA/0.4 nm HATCN in dark and under simulated solar irradiation, as indicated, for the (a) SECO, (b) valence, and (c) zoomed valence regions; also perovskite-background (BGS) subtracted spectra are shown to highlight the HATCN HOMO and SOMO features. Schematic energy-level diagrams (d) in the dark and (e) under 1.5 sun irradiation. The indicated energy values are given with respect to E_F set to zero. The blue dashed lines in (e) represent the quasi-Fermi levels $E_{F,n}$ and $E_{F,p}$ for electrons and holes, respectively; the red arrows and numbers indicate the illumination-induced change of the HATCN energy levels with respect to those of the perovskite.

HATCN is expected to relax in binding energy to the $\text{HOMO}_{\text{anion}}$, but its spectral signature is not sufficiently pronounced to make a clear assignment in the present case. XPS measurements show a constant binding energy of the perovskite Pb 4*f* core levels with respect to E_F before and after HATCN deposition [see Fig. S2(b) in Ref. [24]], revealing that the band positions within the perovskite layer did not change after 0.4 nm HATCN deposition.

Illumination of the PEDOT:PSS/CsFAMA/HATCN (0.4 nm) sample with 1.5 sun during UPS measurements leads to a rigid shift of the HATCN-related energy levels by 0.32 eV towards E_F , apparent for the HOMO and $\text{SOMO}_{\text{anion}}$ emission features in Figs. 2(b) and 2(c). This goes in hand with an increase of the SEP [Fig. 2(a)] by the

same amount, thus again pointing to an electrostatic origin of the energy-level shift. The electron affinity and ionization energy of neutral HATCN molecules is thus the same in dark or under illumination. The energy levels of the perovskite layer underneath exhibit a minor shift of less than 0.1 eV towards E_F during sample illumination, as seen from the Pb 4*f* core levels in Fig. S2(b) of the Supplemental Material [24]. These observations provide clear evidence that the energy levels of the organic material, including the first molecular layer in direct contact with the perovskite, experience a substantial realignment with respect to those of the perovskite upon illumination. This is enabled by the weak (physisorptive) electronic coupling between the two components constituting the interface, as otherwise such a re-alignment would not be possible. Furthermore, the presence of photoinduced negative space charge in HATCN is directly observed by the significant increase of emission intensity from SOMO_{anion} feature in Fig. 2(c). Another interesting observation is that—in addition to the shifted SOMO_{anion} feature—photoemission at even lower binding energy and extending above E_F is observed under illumination [also Fig. 2(c)]. The shape of this emission resembles a Fermi-Dirac distribution typical of metals, whose center is 0.33 eV above E_F . The elucidation of its origin goes beyond the focus and scope of the present contribution, but future work should investigate whether indeed metal-like free electrons are formed or novel correlated molecular states emerge under this nonequilibrium condition.

The energy-level realignment due to solar irradiation of the molecular (sub)monolayer is in full analogy to that seen for 7 nm HATCN on CsFAMA, only the magnitude is smaller. This can be understood from the fact that electrons transferred to HATCN at the interface can diffuse within the thicker layer, so that overall more space charge can build up under the same light intensity. However, there seems to be a maximum for the level-realignment magnitude at a given light intensity, which is governed by the balance of the interfacial electron generation rate, the interfacial carrier recombination, and the space charge induced level shift as adaptive regulator. This is demonstrated with a 20 nm thick HATCN layer (Fig. S3 of the Supplemental Material [24]), which exhibits a shift of 0.74 eV under 1.5 sun illumination.

Next, model photovoltaic cells consisting of a PEDOT:PSS/CsFAMA/HATCN stack were investigated (details are given in Figs. S4 and S5 of Ref. [24]). Given that the open circuit voltage (V_{OC}) is limited by the energy difference between E_F of PEDOT:PSS and the LUMO of HATCN in this architecture, the obtained V_{OC} of 0.7 V compares very favorably to the E_F -LUMO energy difference measured under illumination for the thick HATCN films, thus underpinning the significance of interfacial energy-level realignment under photoexcitation.

To demonstrate that the above identified phenomenon also occurs for other organic semiconductors used in

perovskite-based solar cells, we performed analogous experiments for [6,6]-phenyl-C61-butyric acid methyl ester (PCBM; electron transport material) and 2,2',7,7'-tetrakis [N,N-di(4-methoxyphenyl)amino]-9,9'-spirobifluorene (spiro-OMeTAD; hole transport material) in combination with CsFAMA. Measured in dark, the CsFAMA/PCBM interface exhibits a type-II alignment, with an energy offset of 0.27 eV for electron extraction. Upon sample illumination, a rigid upward shift of the PCBM levels with respect to those of the perovskite by 0.10 eV occurs, lifting the LUMO closer to the perovskite CB. Again, no shift of the Pb 4*f* core levels was observed, regardless of illumination. Thus, electron accumulation in the PCBM layer consistently explains the observations. The corresponding UPS data and energy-level diagrams are shown in Fig. S6 of the Supplemental Material [24].

The deposition of 6 nm spiro-OMeTAD decreases Φ from 5.05 eV (bare CsFAMA) to 4.30 eV (Fig. 3). This is due to Fermi-level pinning induced electron transfer from

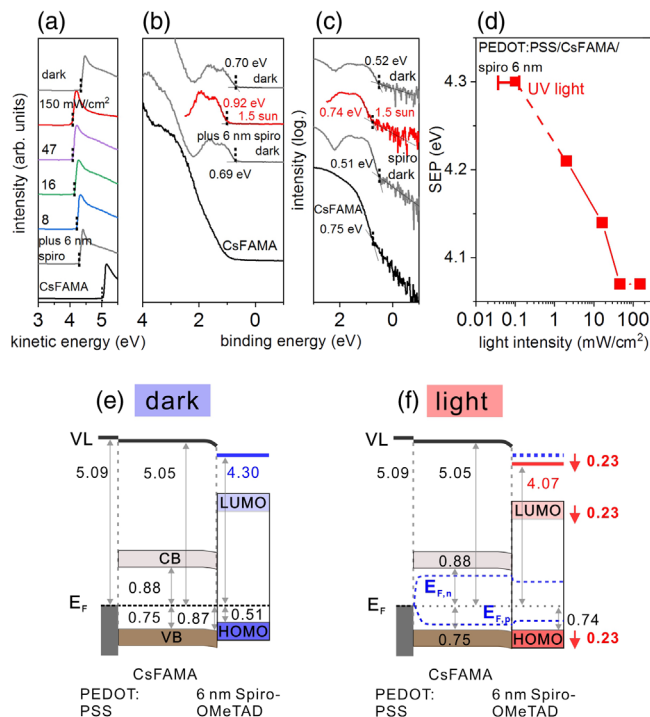


FIG. 3. UPS spectra of PEDOT:PSS/CsFAMA/6 nm spiro-OMeTAD in the (a) SECO, and valence regions (b) on linear and (c) on logarithmic intensity scale, measured under varied simulated solar irradiation (as indicated). (d) SEP measured with respect to the conductive substrate E_F as function of irradiation intensity. Schematic energy-level diagrams (e) in dark and (f) under 1.5 sun irradiation. The spiro-OMeTAD HOMO onset was extrapolated on a logarithmic intensity scale. The indicated energy values are given with respect to E_F set to zero. The blue dashed lines in (f) represent the quasi-Fermi levels $E_{F,n}$ and $E_{F,p}$ for electrons and holes, respectively; the red arrows and numbers indicate the illumination-induced change of the HATCN energy levels with respect to those of the perovskite.

the organic layer to the perovskite because the ionization energy of spiro-OMeTAD is lower than the bare perovskite's Φ . This charge transfer is accompanied by downward surface band bending in the perovskite by 0.12 eV, as observed from the shift of the Pb 4f core levels upon interface formation in Fig. S7 in Ref. [24]. The VB onset of CsFAMA (including the surface band bending determined from XPS) is 0.87 eV and the spiro-OMeTAD HOMO onset is 0.69 eV below E_F [Fig. 3(b)]. The sample SEP now decreases with increasing illumination intensity, down to 4.07 eV at 1.5 sun, as plotted in Fig. 3(d). The SEP change is in the opposite direction to that observed for HATCN and PCBM, consistent with hole accumulation in the hole transport material. The change of the SEP is quantitatively paralleled by a shift of the spiro-OMeTAD HOMO away from E_F by 0.23 eV under 1.5 sun illumination. Importantly, the Pb 4f core levels exhibit no shift between dark and illuminated conditions (see Fig. S7 [24]), i.e., the energy levels of the perovskite remain unchanged.

Finally, we note that HOMO onset extrapolation for organic semiconductors, e.g., for a Gaussian density of states (DOS) distribution, on a linear intensity scale does not account for the small but finite DOS in the Gaussian tail [17,42]. With this method, the spiro-OMeTAD HOMO onset is 0.05 eV below the perovskite VB onset under illumination. In comparison, on a logarithmic scale we find that the HOMO onset 0.13 eV above the perovskite VB, which is more reasonable for a hole-extracting contact. Thus, determination of the perovskites' VB onset (as meanwhile common in the field) and organic semiconductors' level onset on a logarithmic intensity scale may provide a more accurate energy-level determination overall.

In conclusion, we demonstrated that the energy levels at interfaces between three prototypical organic semiconductors and a metal-halide perovskite are not affixed, but free to move under external stimulus. This novel mechanism is based on photoinduced space-charge accumulation in the organic layer and weak electronic coupling between the two compounds forming the interface. Consistently, electron and hole accumulation resulted in shifts of the organic layers' energy levels in opposite direction with respect to those of the perovskite. The magnitude of photoinduced level realignment found with UPS for CsFAMA/HATCN was paralleled by the V_{OC} of a model photovoltaic device, underpinning the practical relevance of this fundamental interfacial phenomenon. If such *operando* energy-level shifts are not accounted for, conclusions from device-level modeling of photovoltaic cells can be misleading for further device-design guidance. The illumination-driven level realignment is expected to occur also at other semiconductor interfaces if weak electronic coupling, a large energy offset for electrons or holes in dark, and sufficient photogenerated carrier density near the interface are present simultaneously. Such "moving" energy levels then have implications for research fields well beyond photovoltaics.

This work was funded by the Deutsche Forschungsgemeinschaft (DFG, German Research Foundation, Projects No. 182087777-SFB951 and No. 423749265-SPP2196 "SURPRISE" and 424394788-SPP2196 "GLIMPSE").

*Corresponding author.

norbert.koch@physik.hu-berlin.de

- [1] J.-H. Im, C.-R. Lee, J.-W. Lee, S.-W. Park, and N.-G. Park, *Nanoscale* **3**, 4088 (2011).
- [2] Y.-H. Lin *et al.*, *Science* **369**, 96 (2020).
- [3] M. Jošt *et al.*, *ACS Energy Lett.* **4**, 583 (2019).
- [4] H.-S. Kim *et al.*, *Sci. Rep.* **2**, 591 (2012).
- [5] <https://www.nrel.gov/pv/cell-efficiency.html>.
- [6] M. Stolterfoht *et al.*, *Energy Environ. Sci.* **12**, 2778 (2019).
- [7] M. Jeong *et al.*, *Science* **369**, 1615 (2020).
- [8] C. M. Wolff, F. Zu, A. Paulke, L. P. Toro, N. Koch, and D. Neher, *Adv. Mater.* **29**, 1700159 (2017).
- [9] P. Schulz, E. Edri, S. Kirmayer, G. Hodes, D. Cahen, and A. Kahn, *Energy Environ. Sci.* **7**, 1377 (2014).
- [10] L. E. Polander, P. Pahner, M. Schwarze, M. Saalfrank, C. Koerner, and K. Leo, *APL Mater.* **2**, 081503 (2014).
- [11] I. Gelmetti, N. F. Montcada, A. Pérez-Rodríguez, E. Barrena, C. Ocal, I. García-Benito, A. Molina-Ontoria, N. Martín, A. Vidal-Ferran, and E. Palomares, *Energy Environ. Sci.* **12**, 1309 (2019).
- [12] Z. Hawash, S. R. Raga, D. Y. Son, L. K. Ono, N. G. Park, and Y. Qi, *J. Phys. Chem. Lett.* **8**, 3947 (2017).
- [13] D. Shin, D. Kang, J. Jeong, S. Park, M. Kim, H. Lee, and Y. Yi, *J. Phys. Chem. Lett.* **8**, 5423 (2017).
- [14] P. Schulz, *ACS Energy Lett.* **3**, 1287 (2018).
- [15] P. Schulz, L. L. Whittaker-Brooks, B. A. MacLeod, D. C. Olson, Y.-L. Loo, and A. Kahn, *Adv. Mater. Interfaces* **2**, 1400532 (2015).
- [16] J. Endres *et al.*, *J. Phys. Chem. Lett.* **7**, 2722 (2016).
- [17] F. Zu *et al.*, *J. Phys. Chem. Lett.* **10**, 601 (2019).
- [18] F. Zu, P. Amsalem, M. Ralaifarisoa, T. Schultz, R. Schlesinger, and N. Koch, *ACS Appl. Mater. Interfaces* **9**, 41546 (2017).
- [19] S. Olthof and K. Meerholz, *Sci. Rep.* **7**, 40267 (2017).
- [20] J.-P. Yang *et al.*, *Solar RRL* **2**, 1800132 (2018).
- [21] T. Hellmann, C. Das, T. Abzieher, J. A. Schwenzer, M. Wussler, R. Dachauer, U. W. Paetzold, W. Jaegermann, and T. Mayer, *Adv. Energy Mater.* **10**, 2002129 (2020).
- [22] F.-S. Zu, P. Amsalem, I. Salzmann, R.-B. Wang, M. Ralaifarisoa, S. Kowarik, S. Duhm, and N. Koch, *Adv. Opt. Mater.* **5**, 1700139 (2017).
- [23] F. Zu, C. M. Wolff, M. Ralaifarisoa, P. Amsalem, D. Neher, and N. Koch, *ACS Appl. Mater. Interfaces* **11**, 21578 (2019).
- [24] See Supplemental Material at <http://link.aps.org/supplemental/10.1103/PhysRevLett.127.246401> for details of perovskite sample preparation, inelastic mean free path of electrons, details of device fabrication and characterization, and fundamental band gap of PCBM material, which includes Refs. [25–28].
- [25] M. Saliba *et al.*, *Energy Environ. Sci.* **9**, 1989 (2016).

- [26] M. P. Seah and W. A. Dench, *Surf. Interface Anal.* **1**, 2 (1979).
- [27] M. Stolterfoht, C. M. Wolff, Y. Amir, A. Paulke, L. Perdigón-Toro, P. Caprioglio, and D. Neher, *Energy Environ. Sci.* **10**, 1530 (2017).
- [28] K. Akaike, K. Kanai, H. Yoshida, J. y. Tsutsumi, T. Nishi, N. Sato, Y. Ouchi, and K. Seki, *J. Appl. Phys.* **104**, 023710 (2008).
- [29] H. Yoshida and K. Yoshizaki, *Org. Electron.* **20**, 24 (2015).
- [30] S. Lee, J.-H. Lee, K. H. Kim, S.-J. Yoo, T. G. Kim, J. W. Kim, and J.-J. Kim, *Org. Electron.* **13**, 2346 (2012).
- [31] F. Peña-Camargo *et al.*, *ACS Energy Lett.* **5**, 2728 (2020).
- [32] I. Levine *et al.*, *J. Phys. Chem. C* **125**, 5217 (2021).
- [33] F. Zhang, J. C. Hamill Jr., Y.-L. Loo, and A. Kahn, *Adv. Mater.* **32**, 2003482 (2020).
- [34] A. Kahn, N. Koch, and W. Gao, *J. Polym. Sci. B* **41**, 2529 (2003).
- [35] S. Braun, W. R. Salaneck, and M. Fahlman, *Adv. Mater.* **21**, 1450 (2009).
- [36] H. Ishii, K. Sugiyama, E. Ito, and K. Seki, *Adv. Mater.* **11**, 605 (1999).
- [37] Q.-K. Wang, R.-B. Wang, P.-F. Shen, C. Li, Y.-Q. Li, L.-J. Liu, S. Duhm, and J.-X. Tang, *Adv. Mater. Interfaces* **2**, 1400528 (2015).
- [38] G. W. Kim *et al.*, *Chem. Mater.* **29**, 8299 (2017).
- [39] P. Amsalem, J. Niederhausen, A. Wilke, G. Heimel, R. Schlesinger, S. Winkler, A. Vollmer, J. P. Rabe, and N. Koch, *Phys. Rev. B* **87**, 035440 (2013).
- [40] J.-P. Yang, F. Bussolotti, S. Kera, and N. Ueno, *J. Phys. D* **50**, 423002 (2017).
- [41] S. Winkler, P. Amsalem, J. Frisch, M. Oehzelt, G. Heimel, and N. Koch, *Mater. Horizon* **2**, 427 (2015).
- [42] Y. Nakayama, S. Kera, and N. Ueno, *J. Mater. Chem. C* **8**, 9090 (2020).